Privacy-Preserving Gait Identification via Center-of-Gravity Oscillation Analysis on a Floor-Based Sensing Platform

Ryota Ozaki, Kodai Ito, Mai Kamihori, and Yuichi Itoh, *Member, IEEE*

***Abstract*—The gait-based individual identification has attracted significant attention for its unobtrusive and user-friendly nature; however, many existing approaches rely on image-based sensing, raising serious privacy concerns. To address this problem, we propose a privacy-preserving gait identification system that utilizes a floor-based sensing platform measuring center-of-gravity (CoG) oscillations and weight data during natural walking. The system is designed for simplicity and robustness, consisting of eight load cells, an aluminum frame and plate, A/D converters, voltage modules, and microcomputers. The time-series data are segmented according to the rancho observational gait analysis (ROGA) system, and both time-domain and frequency-domain features are extracted for machine learning-based classification. Experiments with 31 participants under natural walking conditions, including carrying luggage, demonstrated an *F*1-score of 0.918 through stratified fivefold cross validation. Even without weight information, using only CoG oscillations, the system achieved an *F*1-score of 0.817, confirming that distinctive gait signatures are embedded in body sway patterns. Notably, individual differences were pronounced during the foot transition phase. As the system operates solely on low dimensional, abstract CoG and weight data without capturing identifiable features such as facial images or silhouettes, it offers strong privacy protection. Furthermore, it is robust against external variations including lighting, clothing, hairstyle, and personal belongings. These attributes make the proposed system promising for applications in security, healthcare, and marketing, enabling unobtrusive, privacy-preserving identification based on the natural walking behavior.**

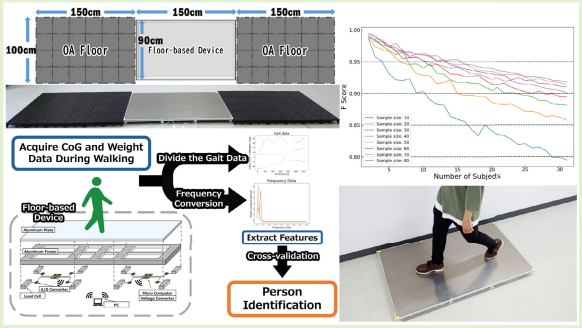

***Index Terms*— Center-of-gravity (CoG) oscillation, floor-based device, gait identification, machine learning, privacy preserving.**

NOMENCLATURE

T_{LR}	Duration ratio of loading response (LR) to total walking time length.
T_{PSw}	Duration ratio of pre-swing (PSw) to total walking time length.
$L_{X,\mathrm{LR}}$	Trajectory length of center-of-gravity (CoG) position X during LR
$L_{Y,\mathrm{LR}}$	Trajectory length of CoG position Y during LR
$L_{Y,\mathrm{MSt}}$	Trajectory length of CoG position Y during mid stance (Mst).
$L_{Y,\mathrm{PSw}}$	Trajectory length of CoG position Y during PSw PSD.
$L_{Y,\mathrm{Swing}}$	Trajectory length of CoG position Y during swing phase.
$\mu_{X,\mathrm{LR}}$	Mean of CoG position X during LR.
$\mu_{Y,\mathrm{LR}}$	Mean of CoG position Y during LR.
$\mu_{W,\mathrm{LR}}$	Mean of total weight W during LR.
$\sigma_{W,\mathrm{LR}}$	Standard deviation of total weight W during LR.
$\sigma_{X,\mathrm{MSt}}$	Standard deviation of CoG position X during MSt.
$\sigma_{W,\mathrm{MSt}}$	Standard deviation of total weight W during MSt.
$\mu_{Y,\mathrm{TSt}}$	Mean of CoG position Y during TSt.

Received 1 August 2025; revised 15 September 2025; accepted 19 September 2025. This work was supported by the Japan Society for the Promotion of Science (JSPS) KAKENHI under Grant JP24H00745. The associate editor coordinating the review of this article and approving it for publication was Dr. Xiao Xu. *(Corresponding author: Ryota Ozaki.)*

This work involved human subjects or animals in its research. Approval of all ethical and experimental procedures and protocols was granted by the Ethical Review Committee of Aoyama Gakuin University.

Ryota Ozaki and Mai Kamihori are with the Graduate School of Science and Engineering, Aoyama Gakuin University, Sagamihara 252-5258, Japan (e-mail: ozaki.ryota@x-lab.team; mai.kamihori@x-lab.team).

Kodai Ito and Yuichi Itoh are with the College of Science and Engineering, Aoyama Gakuin University, Sagamihara 252-5258, Japan (e-mail: kodai.ito@it.aoyama.ac.jp; itoh@it.aoyama.ac.jp).

Digital Object Identifier 10.1109/JSEN.2025.3616782

$\sigma_{W,\mathrm{TSt}}$	Standard deviation of total weight W during TSt.
$\sigma_{X,\mathrm{PSw}}$	Standard deviation of CoG position X during PSw.
$\mu_{W,\mathrm{PSw}}$	Mean of total weight W during PSw.
$\sigma_{W,\mathrm{PSw}}$	Standard deviation of total weight W during PSw.
$\mu_{X,\mathrm{Swing}}$	Mean of CoG position X during swing phase.
$\sigma_{X,\mathrm{Swing}}$	Standard deviation of CoG position X during swing phase.
$\mu_{Y,\mathrm{Swing}}$	Mean of CoG position Y during swing phase.
$\sigma_{Y,\mathrm{Swing}}$	Standard deviation of CoG position Y during swing phase.
$\sigma_{W,\mathrm{Swing}}$	Standard deviation of total weight W during swing phase.
$\mathrm{Width}_{\mathrm{Step}}$	Step width between first and second steps.
$\sigma_{Y,\mathrm{Single}}$	Standard deviation of CoG position Y during single support.
V_{Shift}	Ratio of first-to-second step transition speed to walking speed.
$R_{\mathrm{Heel,Toe}}$	Ratio of heel-to-toe contact time.
P_X	Maximum power in power spectral density (PSD) of CoG position X.
P_Y	Maximum power in PSD of CoG position Y.
P_W	Maximum power in PSD of total weight W.
C_X	Spectral centroid of PSD of CoG position X.
C_Y	Spectral centroid of PSD of CoG position Y.
C_W	Spectral centroid of PSD of total weight W.
BW_X	Spectral bandwidth of PSD of CoG position X.
BW_Y	Spectral bandwidth of PSD of CoG position Y.
BW_W	Spectral bandwidth of PSD of total weight W.
F_X	Spectral flatness of PSD of CoG position X.
F_Y	Spectral flatness of PSD of CoG position Y.
F_W	Spectral flatness of PSD of total weight.

I. Introduction

THE identification of individuals is a fundamental task in modern society, with applications ranging from security and access control to healthcare and marketing. Traditional methods, such as official IDs, PIN codes, and passwords, whereas effective, are often time-consuming and susceptible to loss, theft, or forgery. To address these problems, biometric authentication methods—such as fingerprint, iris, and facial recognition—have been widely adopted, offering seamless and loss-resistant alternatives [17], [18], [31], [40].

Among various biometric modalities, gait-based identification has attracted significant attention due to its unobtrusive and user-friendly nature [12], [33], [48]. Gait, the pattern of limb movements during locomotion, inherently captures both static and dynamic individual traits, such as body structure and walking rhythm. Unlike other biometric methods, gait recognition can operate without requiring active user cooperation, allowing identification to occur naturally as individuals move through monitored spaces. Moreover, because gait is difficult to imitate or disguise, it has been applied in forensic science, with systems developed for criminal investigations [14], [38], and accepted as valid evidence in court trials in U.K. and Denmark [4], [24], [26], [34].

Despite these advantages, most existing gait identification systems rely heavily on image-based sensing technologies, such as RGB cameras and depth sensors [14], [27]. Whereas these approaches can achieve high recognition accuracy, they pose substantial privacy concerns by capturing identifiable visual information, including facial features and body silhouettes. In addition, image-based systems are sensitive to environmental factors such as lighting conditions, clothing variations, and occlusions, which compromise their robustness in real-world deployments. Although alternative approaches employing wearable devices or wireless signals have been explored, they often introduce practical challenges such as the need for continuous wearing, user burden, and strict environmental requirements [50], [56].

To overcome these limitations, floor-based sensing platforms have emerged as a promising alternative. Techniques using sensors embedded in floors [21], [37], [44], seats [3], and insoles [59] have been proposed for unobtrusive gait analysis. By measuring parameters, such as ground-reaction forces and center-of-gravity (CoG) oscillations, these systems offer a privacy-preserving approach without capturing identifiable visual information. In particular, CoG oscillation patterns provide a low dimensional and abstract representation of gait, significantly mitigating at the cost of privacy risks while retaining discriminative power.

CoG and weight data are inherently low-dimensional and abstract, which not only reduces the risk of privacy violations but also minimizes user burden by enabling identification simply by walking over the sensing platform. Moreover, unlike image sensor-based methods, which are influenced by factors such as clothing, hairstyle, camera angle, and ambient lighting, [13], [15], [58], CoG and weight data are less susceptible to these variations. Floor-based devices can be flexibly deployed to suit diverse scenarios and are expected to find applications in areas such as medical examination support, suspicious person detection in office environments, and human flow analysis in public spaces.

In this study, we propose a privacy-preserving gait identification system utilizing a floor-based sensing platform that captures CoG oscillations and weight data during natural walking. We analyzed the data obtained from the device and proposed a method for individual identification using machine learning based on time-domain and frequency-domain features extracted from gait.

As an off-the-shelf, currently, commercial force plates (such as [45]) are available and have demonstrated utility in gait analysis [7], [30], although their high unit cost renders deployment in households and small facilities impractical; therefore, low-cost configurations for floor-based gait analysis are desirable.

In our study, we define “privacy preserving” as a design choice whereby, even in the incident of unintended data disclosure (e.g., due to external attack or operational error), the recorded data do not readily enable direct reidentification of specific individuals from human-interpretable appearance cues (e.g., face and silhouette/body shape). Vision-based methods (e.g., camera systems), while accurate, inherently tend to include such content and therefore carry a relatively higher

risk of reidentification upon leakage. In contrast, the CoG and weight signals used in this study are nonvisual and low dimensional, making it difficult for humans to interpret the raw data alone and link them to a specific individual.

In addition, our floor-based device acquires these signals only when a pedestrian traverses a confined sensing area (1.5×0.9 m and 1.35 m^2), which reduces the incidental capture of bystanders and lowers the reidentification risk structurally relative to wide-FOV camera systems.

Furthermore, we investigate the impact of carrying luggage, jackets, and accessories on gait-based identification, aiming to establish a robust, general-purpose system resilient to variations in carried weight. We also examine the feasibility of enhancing privacy by evaluating system performance when excluding weight data. The principal contributions of this article are summarized as follows.

1) *Low-Cost, Low-Density Platform:* We developed a floor-based sensing platform that captures low dimensional, abstract CoG oscillations and weight data, without visual input. Unlike high-density pressure mats [43] or commercial costly force plates [45], our platform uses only eight load cells mounted on a 150×90 cm aluminum plate; however, it identifies 31 individuals under natural walking conditions with an $F1$-score exceeding 0.90. Our approach adopts a low-density sensor configuration that is less susceptible to the calibration and maintenance burdens [8], [19], [57] inherent to high-density designs, and despite the simplified hardware, achieves performance comparable to these prior works, particularly in small-cohort settings.
2) *Interpretable Gait-Phase Features:* Using rancho observational gait analysis (ROGA) to segment the gait cycle, we clarify how phasewise changes in weight and CoG trajectories capture individual-specific patterns useful for individual identification. Permutation-importance analysis suggested relatively strong contributions from the features derived from the LR and PSw phases. To the best of our knowledge, we have not confirmed prior work that has combined CoG/weight signals with ROGA-aligned phase segmentation and quantitatively assessed feature contributions.
3) *Robustness to Real-World Occlusions:* We demonstrate that identification accuracy remains virtually unchanged when participants carry luggage—an occlusion scenario that degrades both camera-based and existing floor-sensor methods [25], [53], [60]—highlighting the robustness of the system to everyday environmental variations. Using board-level CoG/vertical load with ROGA-aligned, z-standardized relative-oscillation features, the system absorbs offsets from carried luggage, keeping identification accuracy virtually unchanged under carried-object conditions ($F1 = 0.918$ in our dataset).
4) *Privacy-Oriented CoG-Only Mode:* We further show that CoG oscillations data alone, without weight information, retain sufficient discriminative power. Although the accuracy drops slightly, the CoG-only mode still exceeds 90% for cohorts of roughly ten users, suggesting an even more privacy-preserving biometric recognition method.

II. Related Works

A. Gait Analysis

Numerous studies have focused on gait-based identification for individuals and attribute classification, such as age and gender. However, the majority of these studies have employed image-based sensing modalities, including RGB and depth sensors. Makihara et al. [27] utilized 25 cameras to capture gait data and demonstrated that pedestrians could be classified into four categories: children, adult men, adult women, and elderly individuals. Iwama et al. [15] constructed the world's largest gait database and reported that recognition performance was higher for women than for men, and that gait characteristics change with growth and aging. Randhavane et al. [39] proposed an emotion classification algorithm based on RGB walking images, achieving an accuracy of 80.07%. Xia et al. [54] employed a time-of-flight (ToF) sensor to capture time-series walking data and achieved an average identification accuracy of 91.05% for ten users by segmenting the data into intervals for analysis. Wang et al. [49] collected gait data from 43 depressed and 52 nondepressed patients using Kinect, proposing a real-time automatic depression detection framework.

Whereas gait-based identification often achieves high accuracy and demonstrates the utility of gait as a biometric modality, camera-based approaches are highly susceptible to environmental and user-related factors, including lighting conditions, clothing, hairstyle, and viewing angle [13], [15], [58]. For instance, Xu et al. [55] demonstrated that recognition accuracy significantly decreased when pedestrians were captured from frontal or rear views compared to side views, and that certain hairstyles could cause adults to be misclassified as children. Moreover, video footage obtained via cameras inherently contains sensitive personal information such as skeletal structures and facial features, raising substantial privacy concerns. A user survey conducted by Laput et al. [23] revealed that a significant proportion of participants were reluctant to engage with camera-based systems due to privacy risks. In addition, according to a survey by Seymour et al. [42], camera-based surveillance can elicit unconscious responses in social-vision mechanisms and a felt sense of being watched, even when explicit awareness is minimal or merely implied, suggesting a potential psychological burden of surveillance.

Despite these challenges, the gait analysis remains widely employed in criminal investigations and surveillance, where high accuracy is prioritized over privacy concerns [14], [27], [38]. However, for applications such as human flow analysis, household use, and small office environments, it is essential to develop methods that maintain recognition accuracy while mitigating privacy risks.

To address these concerns, alternative methods that do not rely on cameras have been explored. Xu et al. [56] extracted gait information from acoustic signals captured by a commercial acoustic device and achieved 96.6% accuracy in identifying 50 individuals. Wang et al. [50] utilized commercial Wi-Fi routers and laptops to measure gait, reporting an accuracy

of 93.05% for 50 users. Nakamura et al. [32] employed an AdaBoost classifier to detect steps from floor-mediated vibration signals and argued that the resulting step patterns might embed person-specific signatures. Dong and Noh [9], by continuously recording gait-induced vibrations with floor-mounted sensors, estimated spatiotemporal parameters—step time/length and stance/swing width/angle—with root-mean-square errors of 0.08 s and 0.38 m, respectively; health-related metrics such as cadence and bilateral symmetry were predicted with an RMSPE of 7.7%. However, these signal-, sound-, and vibration-based methods require strict environmental conditions to maintain high accuracy, facing limitations due to device placement constraints, interference from external signals, and sensitivity to variations in clothing styles.

Wearable-device-based approaches have also been investigated. Fujii et al. [10] developed a slipper-type device equipped with an accelerometer that achieved 95.0% accuracy for discriminating five individuals. Other studies have explored the use of acceleration and inertial sensors embedded in smartphones for user identification [11], [22]. Whereas wearable devices offer advantages such as improved privacy protection and lower installation costs compared to camera-based systems, they impose practical challenges, including the need for continuous wearing, battery depletion, and user discomfort.

B. Sensing by Pressure and Load Data

In contrast, pressure- and load-based sensing platforms have emerged as promising privacy-conscious alternatives. These approaches capture weight and pressure variations during walking, providing low-dimensional and abstract data that inherently reduce the risk of privacy violations. Orr and Abowd [36] introduced an early floor sensor capable of measuring foot contact and lift-off timing, achieving 93% identification accuracy for 15 individuals, though it remained unclear whether the observed performance reflected natural gait patterns. Middleton et al. [29] proposed a low-cost floor-sensor array with 1,536 pressure sensors and reported approximately 80% accuracy for individual identification. Yoshida et al. [57] developed a modular floor interface capable of touch inference, tracking, and foot gesture recognition. Shi et al. [43] developed a smart floor monitoring system using high sensor-density friction electric sensors embedded in a mat, achieving 96.0% accuracy in identifying ten participants integrated with deep learning base data analysis.

In floor-based sensing that leverages ground-reaction forces, many studies have employed high-density sensor arrays. Although dense layouts can capture detailed spatial pressure distributions and often achieve high accuracy, they also scale up the calibration points, wiring complexity, and potential failure sites. Prior studies have reported practical issues, such as the cost of long-term drift requiring in situ recalibration, as well as the labor associated with fault detection and sensor replacement when elements degrade [8], [19]. Several studies have proposed countermeasures; for example, Yoshida et al.'s [57] *Flexel* implements automatic detection and compensation for failed elements, and Mei et al. [28] improved per-channel linearity in dense arrays to alleviate the calibration burden. Taken together, these observations indicate that calibration and maintenance may be recurring concerns in high-density floor systems, highlighting the relevance of low-density designs in scenarios in which ease of deployment and upkeep are critical.

Other studies have extended the use of weight and CoG data. Ozaki et al. [37] used CoG and weight data collected during walking, standing, and sitting—not truly natural gait—to evaluate frailty conditions in elderly individuals without imposing burdens on the participants, although it did not target individual identification. Bränzel et al. [5] employed pressure images captured by cameras installed beneath the floor to infer furniture layout, user position, posture, and certain airborne events. Arnrich et al. [3] analyzed seated pressure data to recognize stress and cognitive load states. Kitabayashi et al. [21] measured body sway in 1107 individuals and demonstrated the ability to distinguish between different age groups and assess physical condition. Nishimura et al. [35] utilized a "SenseChair" equipped with four pressure sensors under the seat to detect nodding with an accuracy comparable to camera-based methods and found a positive correlation between nodding frequency and intellectual productivity during group discussions. Yu et al. [59] developed a shoe-type device embedding a pressure sensor in the insole, capable of tracking walking paths with an average positional error of less than 1.05 m, even when participants were carrying luggage, suggesting the robustness of gait-based feature analysis under load variations.

These studies collectively demonstrate that individuals' movements and physical states can be effectively inferred from variations in weight and pressure exerted on floor or seat surfaces. Although the pressure and weight data are inherently low-dimensional and abstract, they encompass sufficient information to support individual and attribute recognition without compromising user privacy.

Building on this premise, we developed a gait analysis system incorporating a floor-based device designed to leverage weight and CoG data collected during natural walking for individual identification. Our approach involves measuring weight distribution and CoG oscillations during gait cycles and extracting features based on traditional gait analysis techniques widely used in physical therapy and related disciplines. Furthermore, we explore the feasibility of achieving reliable identification using only CoG oscillation data, evaluating whether body sway alone, without explicit weight information, provides sufficient discriminatory power.

III. Proposed Method

A. Floor-Based Device

We propose a privacy-preserving gait analysis system that comprises a floor-based sensing platform to measure CoG oscillations and weight data during natural walking, along with a data acquisition and analysis program. Fig. 1 illustrates the overall system architecture, while Fig. 2 shows the floor-based device with a person walking on it.

Based on the prior work [59], the average human stride length is approximately 72.60 cm. To ensure that at least two steps can be captured, we designed the long side of the device to be 150 cm, which exceeds twice the stride length

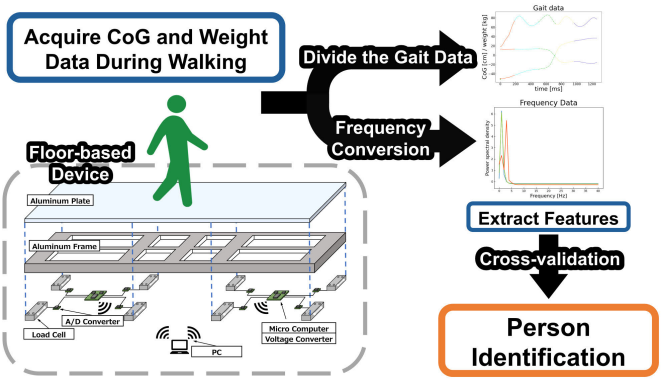

Fig. 1. Overview of the proposed system.

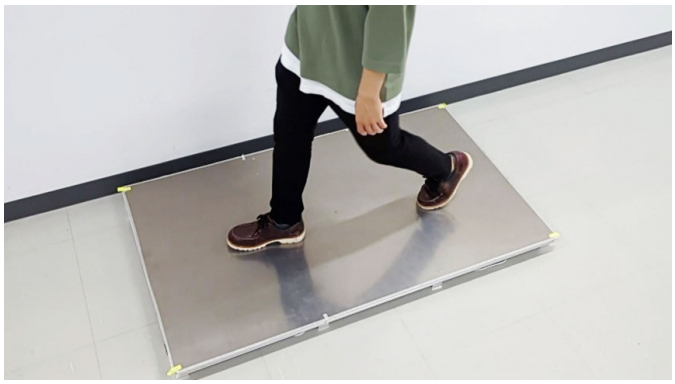

Fig. 2. Floor-based device.

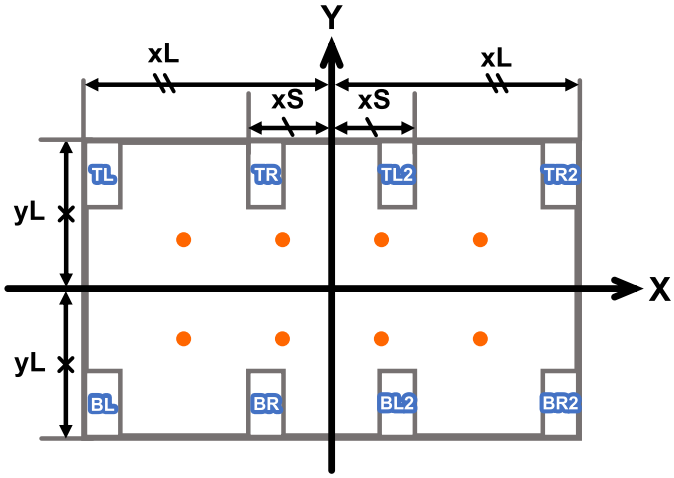

Fig. 3. Arrangement of the eight load cells. The orange dots indicate the grid points used to evaluate the CoG measurement accuracy.

(145.20 cm). The platform consists of 11 aluminum frames, an aluminum plate, eight load cells, eight A/D converters, four voltage conversion modules, and two microcomputers.

Each load cell (LCB03-K060L, A&D Company [2]) has a rated capacity of 61.18 kg and is paired with an A/D converter. Voltage conversion modules are included to adjust the signal levels between the load cells and microcomputers. We employ ESP32-DevKitC boards, featuring the ESP-WROOM-32 module with integrated Wi-Fi capability, to enable wireless data transmission. Four load cells are symmetrically positioned at the four corners, and the remaining four are positioned at 50-cm intervals along the long sides, dividing them into three equal segments. Only the load cells make contact with the floor surface.

B. Calculation of CoG and Weight Data

The weight data are acquired from the eight load cells at a sampling rate of 80 Hz. The total weight is computed as the sum of the load cell measurements. The device's center is designated as the origin, the long side is aligned along the X-axis in the walking direction (front–back), and the short side is aligned along the Y-axis (left–right). CoG coordinates are calculated based on the load cell readings and their respective distances from the origin. As illustrated in Fig. 3, the vertical loads measured by the individual load cells are denoted by TL, TR, BL, BR, TL2, TR2, BL2, and BR2. Using the distances from the origin to each load cell, the total weight W and the CoG coordinates X and Y can be expressed by the following equations:

$$W = \mathrm{TL} + \mathrm{TR} + \mathrm{TL2} + \mathrm{TR2} + \mathrm{BL} + \mathrm{BR} + \mathrm{BL2} + \mathrm{BR2} \tag{1}$$

$$x = \times \frac{(-\mathrm{TL}-\mathrm{BL}+\mathrm{TR2}+\mathrm{BR2})xL+(-\mathrm{TR}-\mathrm{BR}+\mathrm{TL2}+\mathrm{BL2})\times xS}{W} \tag{2}$$

$$Y = \times \frac{(\mathrm{TL}+\mathrm{TR}+\mathrm{TL2}+\mathrm{TR2})\times YL+(\mathrm{BL}+\mathrm{BR}+\mathrm{BL2}+\mathrm{BR2})\times(-yL)}{W}. \tag{3}$$

C. CoG Measurement Evaluation

We assessed the spatial resolution of the floor-based device implemented in this study. For ease of coordinate management, the lower left corner of the platform was set as the origin (0, 0). An 8444 ± 3 g mass was placed for 5 s on each of the eight points arranged on a 300-mm grid, and the procedure was repeated five times per point.

Fig. 4 shows the pointwise and overall RMSE values. The largest error, 1.64 mm, occurred at (300, 600)mm, while the overall mean RMSE was 0.65 mm. The likely sources of error include a slight misalignment during sensor installation, floor unevenness beneath the device, and minute placement offsets of the test mass. Even the maximum error of 1.64 mm is negligible relative to the platform's 1500 × 600 mm dimensions and is therefore considered well within practical tolerance. Moreover, our identification pipeline utilize relative CoG variations; all features are standardized within the training set. Consequently, an error of this magnitude is expected to have only a minimal effect on the system accuracy.

D. Data Preprocessing

First, the walking intervals are extracted from the time-series data. We determined that the CoG is reliably measured when the total weight on the device exceeds approximately one-fourth of the user's body weight. Consequently, we exclude samples with a total weight below 15 kg, based on an average adult weight of 62 kg [47], and samples, where the CoG position lies outside the device's bounds.

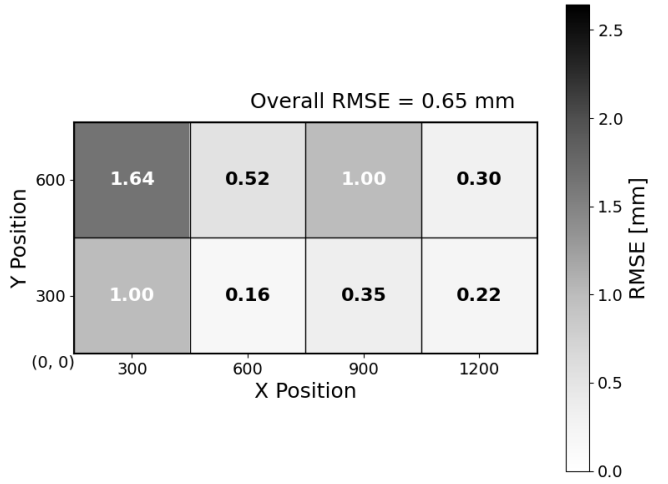

Fig. 4. Heat map of the CoG measurement error. Values indicate the RMSE (mm) at each 300-mm grid point.

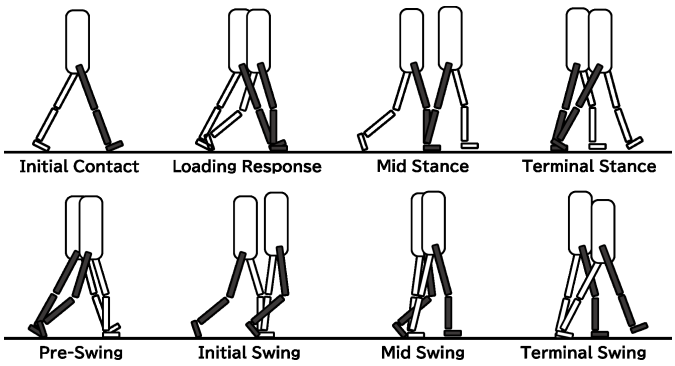

Fig. 5. Eight phases within a gait cycle redrawn from [16].

Next, to synchronize data from two microcomputers, the time-series data are resampled uniformly at 80 Hz. Given that this sampling rate is sufficiently high for measuring human movements, resampling does not cause significant data loss. A moving average filter is subsequently applied to reduce noise.

E. Feature Extraction

1) Time-Domain Features: The preprocessed CoG and weight data are segmented based on the ROGA system [1], widely used in physical therapy. The ROGA is frequently cited in the literature and has been developed to assess gait patterns in a wide range of patients [46]. It also clearly defines reference points for segmenting the normal gait cycle of healthy individuals unaffected by the disease. Therefore, in this article, we reference ROGA and segment the measured CoG and weight data based on the description in [16].

Fig. 5 shows the eight phases of the walking cycle as defined in [16]. Initial contact (IC) occurs when the heel of the first step contacts the ground, and LR spans from IC until the rear foot lifts off. Mst follows LR and continues until the heel of the front foot lifts off. The period from then until the IC of the second step is terminal stance (Tst).

After TSt, PSw begins when the first foot leaves the ground, and initial swing (ISw) occurs when that foot crosses over the second foot in the air. Mid swing (MSw) follows, extending until the first foot is perpendicular to the ground. The period until the next cycle's IC is terminal swing (TSw). Humans repeat these phases seamlessly, with each phase's endpoint (except IC) marking the next phase's start. In the gait cycle, the stance phase runs from IC to PSw, the swing phase from ISw to TSw, and the single support phase from MSt to TSt.

The measured CoG and weight data were segmented according to the following procedure. Fig. 6 illustrates an example of the time-series data after segmentation. First, the starting point of the data was defined as the moment when the first foot made contact with the device, which was configured as IC, and the starting point for LR. Next, the moment when the average weight in the data was exceeded for the first time was defined as the point when the rear foot left the floor, marking the endpoint for LR and the starting point for MSt.

We identified the pair of poles with the maximum movement speed among the poles on the Y-axis of the CoG, and determined that the interval between these poles corresponded to the period during which the CoG shifted from one foot to the other. The first pole of the pair was considered to represent the moment when the weight was fully transferred to the first foot, specifically, when the heel of the first foot left the ground. This point was configured as the endpoint of the MSt and the starting point of the TSt. The second pole of the pair represents the moment when the weight was fully transferred to the second foot, that is, when the first foot left the ground. This point was set as the endpoint for PSw and the starting point for ISw. The midpoint of these poles along the time axis was defined as the IC of the second step, marking the endpoint of TSt and the starting point of PSw.

This process can detect the interval between the first and second steps for a sample that takes two steps on a device, such as that shown in Fig. 6. However, it may misidentify the steps for samples that involve three or more steps. Because the floor-based device in this study had a limited area, it was necessary to extract features from the first step that were consistent across all walking samples.

Therefore, z-scores and quantile scores were calculated for the speed of movement between all the poles of each sample, and the pair with the largest speed of movement compared to the other pairs, as well as the most forward in the time series, was selected. In this way, features were extracted from the first step range, regardless of the number of steps taken.

The floor-based device is designed for a minimum of two steps, in which case, the third step lands outside the device. Therefore, we decided that it would be difficult to divide the phases after the ISw and integrate them into one phase as the swing phase.

From each gait phase, we extract the following time-domain features.

1) Duration ratios relative to total walking time.
2) Trajectory lengths of CoG positions in the X- and Y-axes.
3) Means and standard deviations of CoG positions (X, Y) and total weight (W).

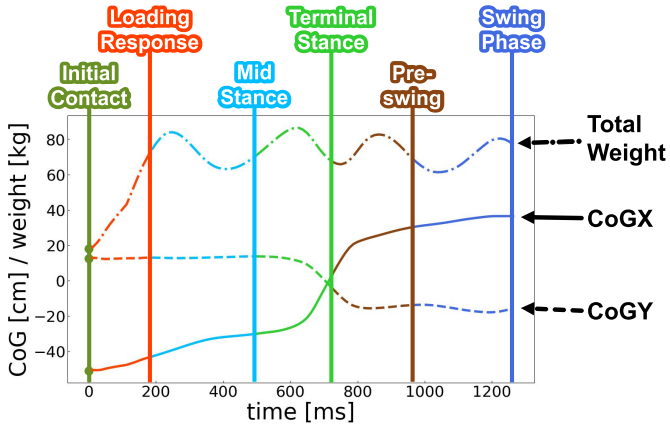

Fig. 6. Example of time-series data divided into each phase of the gait cycle.

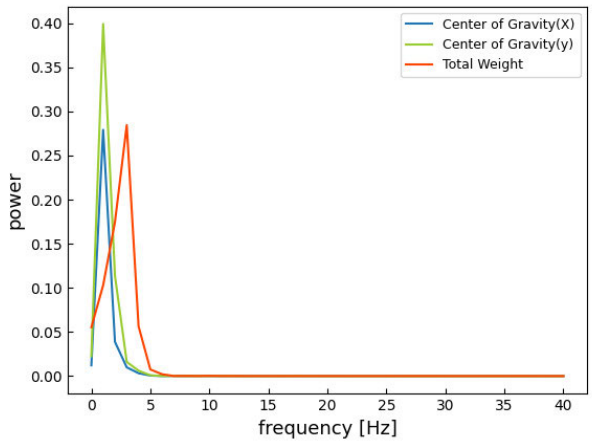

Fig. 7. Example of plotting of power spectrum. This plot shows that the dominant energy lies below 10 Hz.

The trajectory length is defined as the coordinates of the CoG of the ith data as $A_i\left(m \leq i \leq n\right)$, and the operation to find the trajectory length is defined as the function $L(A)$, as in the following equation:

$$L\left(A\right) = \sum_{i=m}^{n-1} \left|A_{i+1} - A_i\right|, \quad A \in X, Y \tag{4}$$

where the trajectory lengths of the CoG positions in the X- and Y-directions are represented by $L(X)$ and $L(Y)$, respectively.

Furthermore, we calculated the characteristics of the duration ratio, stride length, and step distance between the first and second steps, as we believed that these characteristics would also be reflected. In ROGA, the stride length is defined as the distance between the heels of the first and second steps [16]. In this study, we adopted this definition and calculated the time-length ratio and stride length from the interval between the IC, the moment when the first foot made contact with the device, and the starting point of PSw, defined as the moment when the second foot touched the ground. The stride length was measured as the trajectory length of the CoG in the X-direction during this interval. The step width is calculated as the trajectory length of the CoG position in the Y-direction, from the start of TSt (the extreme point on the Y-axis) to the end of PSw, to characterize the spread between the left and right feet.

Furthermore, to capture the stability during the period when the body is supported by one leg, we extracted the time-length ratio of the one-leg support period to the total duration of the data, along with the CoG positions in the X- and Y-directions, and the standard deviation of the total weight (W) as characteristic features.

In addition, considering that the force during the moment of stepping off is characteristic, the force product with respect to time in TSt, the phase when the footsteps off, and the next foot is moved forward in ROGA, is used as a feature value. The speed of moving the next foot to the ground is assumed to change based on the stepping-off force, and the ratio of the speed of movement from TSt to PSw to the total speed of the entire dataset is used as a feature value.

Middleton et al. [29] reported that the accuracy of individual identification improved when the heel-to-toe ratio contact time was used as a feature. Therefore, this feature is used in this study. In this article, we defined LR as the interval when only the heel made contact with the ground, and TSt as the interval when only the toe made contact.

2) Frequency-Domain Features: This article assumed that gait characteristics are expressed by the frequency components of the CoG position in the X- and Y-coordinates, as well as the total weight, during walking. A frequency transformation was applied to the preprocessed CoG and weight data using the Welch method [51] with a Hamming window (window length: 80 samples and 50% overlap), resulting in a frequency resolution of 1 Hz. Frequency features are then extracted based on the output PSD. In an experiment by Sejdić et al. [41], it was reported that distinguishing between healthy individuals, patients with Parkinson's disease, and neuropathic patients was difficult using typical spatiotemporal features, such as mean stride length and the coefficient of variation of stride length. However, using frequency features, they were able to distinguish between these groups, indicating that frequency analysis is useful for gait analysis. Because human gait is a cyclic behavior, we believe that gait characteristics can be effectively expressed in terms of frequency; thus, we adopted frequency features for this study.

Fig. 7 shows that both the CoG position and total weight exhibit strong power below 5 Hz, with the power dropping to almost 0 after 10 Hz. Therefore, to extract features from the frequency range where the power is most prominent, features are extracted from the range below the third quartile frequency in the PSD power distribution.

The maximum power in the PSD was extracted to capture the strongest frequency components in the CoG and the weight data during walking. Next, we extracted the spectral centroid of gravity, which indicates that the location of the PSD is particularly concentrated also within a limited frequency range. The spectral centroid was larger when the PSD was biased toward high-frequency components and smaller when it was biased toward low-frequency components. The spectral CoG spans the range up to the nth frequency corresponding

to the third quartile. When the ith PSD and frequency are denoted by $\mathrm{PSD}_{A,i}$ and $f_{A,i}\left(1 \le i \le n\right)$, respectively, the operation to compute the spectral CoG is defined as function $C(A)$, as shown in the following equation:

$$C\left(A\right) = \frac{\sum_i \mathrm{PSD}_{A,i} f_{A,i}}{\sum_i \mathrm{PSD}_{A,i}}, \quad A \in X, Y, W \tag{5}$$

where the spectral centroid of the CoG positions in the X- and Y directions and total weight (W) are represented by $C(X)$, $C(Y)$, and $C(W)$, respectively.

Subsequently, the spectral bandwidth was extracted as a feature. The spectral bandwidth indicates whether the PSD is concentrated around a particular frequency. A smaller value indicates that the PSD is biased toward a specific frequency, whereas a larger value suggests that the PSD is spread across a wider range of frequencies. When targeting the range up to the nth frequency corresponding to the third quartile, and with the ith PSD and frequency denoted as $\mathrm{PSD}_{A,i}$ and $f_{A,i}\left(1 \le i \le n\right)$, the operation to calculate the spectral bandwidth is defined as the function $\mathrm{BW}(A)$, as shown in (6):

$$\mathrm{BW}\left(A\right) = \left(\frac{\sum_i \mathrm{PSD}_{A,i}\left(f_{A,i} - C(A)\right)^2}{\sum_i \mathrm{PSD}_{A,i}}\right)^{\frac{1}{2}}, \quad A \in X, Y, W \tag{6}$$

where the spectral bandwidths of the CoG positions in the X- and Y-directions, and total weight (W) are denoted by $\mathrm{BW}(X)$, $\mathrm{BW}(Y)$, and $\mathrm{BW}(W)$, respectively.

Finally, the spectral flatness is calculated and used as a feature. The spectral flatness is calculated on a scale from 0 to 1, with a value closer to 1 indicating a uniformly spread PSD and a value closer to 0 indicating a PSD biased toward a particular frequency. When the range extends up to the nth frequency corresponding to the third quartile and the ith PSD is denoted by $\mathrm{PSD}_{A,i}\left(1 \le i \le n\right)$, the operation to calculate the spectral flatness is defined as the function F_A, as shown in the following equation:

$$F\left(A\right) = \frac{\exp\left(\frac{1}{n}\sum_i \ln\left(\mathrm{PSD}_{A,i}\right)\right)}{\frac{1}{n}\sum_i \mathrm{PSD}_{A,i}}, \quad A \in X, Y, W \tag{7}$$

where the spectral flatness of the CoG positions in the X- and Y-directions, and total weight (W) are denoted by $F(X)$, $F(Y)$, and $F(W)$, respectively.

3) Feature Elimination: Although a rich set of features was extracted, some exhibited strong inter-feature correlations, which could potentially lead to multicollinearity. Multicollinearity can increase model complexity, degrade generalization performance, and reduce model interpretability. Therefore, to ensure a parsimonious feature set, we conducted a feature elimination process based on the variance inflation factor (VIF).

VIF is a widely used metric to detect multicollinearity among features, with values greater than 10 indicating a high likelihood of multicollinearity [20]. Initially, VIF values were computed for all features. The feature with the highest VIF was iteratively removed, and the VIFs were recalculated for the remaining features. This elimination process continued until all features had VIF values below 10.

As a result of this procedure, 28 features were excluded, and 39 features were retained as the final input feature set for subsequent classification tasks. The selected time-domain and frequency-domain features are summarized in the Nomenclature.

TABLE I
PARTICIPANT DEMOGRAPHICS

Attribute	Average	SD
Age [years]	22.48	0.80
Height [cm]	164.97	9.50
Weight [kg)]	57.23	10.48
Weight with luggage [kg]	61.21	11.31

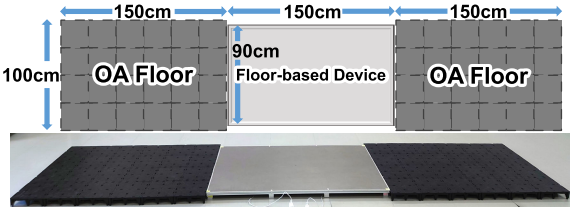

Fig. 8. Experimental setup and walking environment.

IV. EXPERIMENTAL EVALUATION

A. Experimental Setup

Data were collected from 31 undergraduate and graduate students (15 males and 16 females) after obtaining written informed consent. The demographic characteristics of the participants are summarized in Table I. This experiment was conducted under the approval of the Ethical Review Committee of the authors' institution.

To investigate the effect of additional load beyond body weight, participants walked under two conditions: without and with luggage, jackets, and accessories. Each participant performed 40 trials per condition, resulting in 80 trials per participant and a total of 2480 trials across all participants.

The experiment was conducted in a 9 × 7 m room equipped with a continuous walking path using OA flooring (150 × 100 cm) before and after the sensing platform, as shown in Fig. 8. Participants were instructed to walk naturally without intentional alteration of gait, and sufficient practice time was provided before data collection in each condition.

B. Data Scrutiny

The acquired CoG and weight time-series data were visually inspected. Trials with incomplete or erroneous measurements were excluded, yielding 2394 valid walking trials. Features described in the Nomenclature were extracted, with manually set parameters to ensure robust gait phase segmentation.

C. Classification Results

We evaluated identification performance using multiple classifiers: k-nearest neighbors (kNNs), logistic regression, decision tree, linear support vector classifier (SVC), nonlinear SVC with RBF kernel, random forest, AdaBoost, and naive Bayes. Each feature was standardized based on the training data, and a fivefold stratified cross validation was employed. Table II summarizes the results.

Random forest achieved the highest $F1$-score (0.918), followed closely by SVC with RBF kernel (0.915). All evaluation

TABLE II
COMPARISON OF CLASSIFIER PERFORMANCE (STRATIFIED FIVEFOLD CROSS VALIDATION)

Classifier	Accuracy	Precision	Recall	F1-score
k-Nearest Neighbors	0.844	0.855	0.842	0.842
Logistic Regression	0.913	0.917	0.912	0.912
Decision Tree	0.699	0.712	0.698	0.697
SVC (Linear)	0.890	0.894	0.888	0.887
SVC (RBF Kernel)	0.916	0.920	0.915	0.915
Random Forest	**0.919**	**0.922**	**0.918**	**0.918**
AdaBoost	0.816	0.843	0.816	0.821
Naive Bayes	0.840	0.848	0.839	0.838

TABLE III
CLASSIFIER PERFORMANCE AFTER EXCLUDING ONE-STRIDE WALKERS (STRATIFIED FIVEFOLD CROSS VALIDATION)

Classifier	Accuracy	Precision	Recall	F1-score
k-Nearest Neighbors	0.863	0.872	0.860	0.861
Logistic Regression	0.924	0.927	0.923	0.923
Decision Tree	0.732	0.739	0.729	0.728
SVC (Linear)	0.898	0.904	0.897	0.898
SVC (RBF Kernel)	**0.931**	**0.934**	**0.930**	**0.930**
Random Forest	**0.925**	**0.927**	**0.924**	**0.924**
AdaBoost	0.850	0.871	0.850	0.853
Naive Bayes	0.872	0.879	0.871	0.871

metrics were computed using macro-averaging due to the balanced number of trials per participant.

Because the walking path of our floor-based device was limited, the number of steps recorded varied across participants. Specifically, some participants completed one full stride (i.e., an entire gait cycle) on the device, whereas others completed only a single step. To examine whether step count influences identification performance, we removed the eight participants who walked a full stride (2 males, 6 females) and analyzed them using a fivefold stratified cross validation. Table III summarizes the results of each classifier. As a result, SVC with RBF kernel had the highest $F1$-score (0.930), whereas random forest, which was the most accurate classifier when using all participant data, had an $F1$-score of 0.924.

Based on the above results, the proposed method demonstrated a high accuracy in identifying which registered user was walking. However, the evaluation remained insufficient in terms of authentication performance, specifically, the ability to detect and reject unregistered (i.e., unauthorized) users. To address this limitation, we computed standard biometric authentication metrics, including the receiver operating characteristic (ROC) curve, area under the curve (AUC), and equal error rate (EER), to assess the open-set authentication capability of the system. The evaluation was conducted by withholding a subset of the participants from the training data and treating them as unknown users. We varied the number of excluded users (5, 10, 15, 20, and 25 of the 31 participants) to simulate different levels of unknown user scenarios, and utilized the softmax score. Fig. 9 presents the ROC curves along with the corresponding AUC and EER values. The results showed that the system achieved an average AUC of 0.894 and an EER of 0.185.

1) Impact of Participant and Sample Size: We further examined system performance by varying the number of participants and samples per participant, simulating smaller group

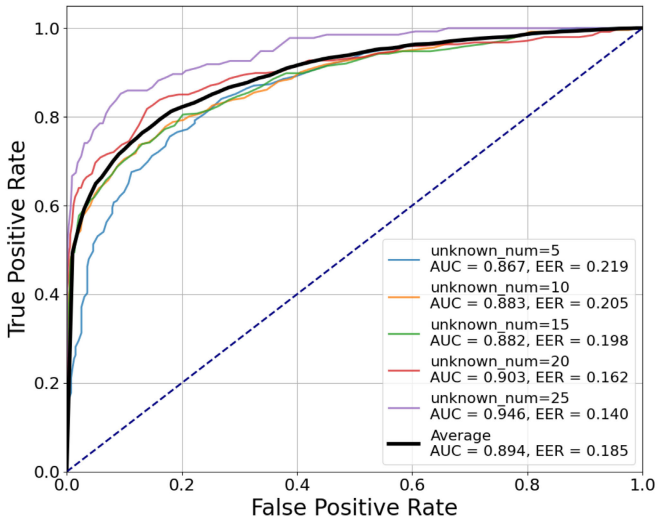

Fig. 9. ROC curves for different numbers of withheld (unknown) users, with AUC and EER results. The dashed diagonal line marks the chance level.

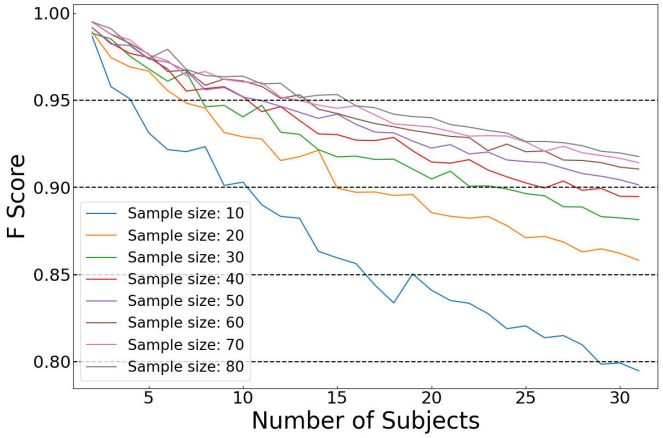

Fig. 10. $F1$-score variation with number of participants and samples per participant.

scenarios such as household environments. Fig. 10 illustrates the $F1$-score trends as the number of participants and sample sizes are varied. To prevent overestimation caused by favorable data pairings, participants and samples were randomly selected for cross validation. This process was repeated 30 times, and the average identification performance was evaluated.

As expected, identification accuracy decreases with fewer samples and more participants, but stabilizes with increased samples. With 80 samples per participant, 15 participants could be identified with an $F1$-score above 0.95. Even with only ten samples per participant, three participants could be identified with an $F1$-score above 0.95 and eight participants with an $F1$-score above 0.90. When identifying 31 individuals, a sample size of 50 per person was sufficient to achieve an $F1$-score above 0.90. For ten individuals, identification with an $F1$-score above 0.90 and 0.95 was possible using 15 and 40 or more samples per user, respectively.

2) Effect of Nonbody Weight Load: Carrying luggage is an external factor that affects gait [12]. Therefore, we compared

TABLE IV
IDENTIFICATION PERFORMANCE WITH AND WITHOUT LUGGAGE

Condition	Accuracy	Precision	Recall	F1-score
Without Luggage	0.917	0.923	0.917	0.915
With Luggage	0.921	0.929	0.919	0.918
Mixed	0.919	0.922	0.918	**0.918**

TABLE V
IDENTIFICATION PERFORMANCE WITH AND WITHOUT WEIGHT DATA

Condition	Accuracy	Precision	Recall	F1-score
With Weight Data	0.919	0.922	0.918	**0.918**
Without Weight Data	0.820	0.824	0.819	0.817

identification results between the luggage and no-luggage conditions. Here, "luggage" encompasses any additional carried load, including bags, jackets, and accessories. The results, shown in Table IV, indicate that the presence of luggage had a negligible impact, with the $F1$-score improving marginally from 0.915 to 0.918.

3) Effect of Excluding Weight Data: To evaluate the feasibility of a more privacy-preserving system, we also tested the performance using only CoG oscillation data, excluding weight information. As summarized in Table V, the $F1$-score dropped by 0.101, from 0.918 to 0.817.

These results suggest that whereas incorporating weight data improves performance, acceptable accuracy can still be achieved using only CoG oscillations, supporting the development of a more privacy-conscious identification system.

V. DISCUSSION

A. Potential of the Proposed Method as an Identification System

1) Individual Identification: We divided the CoG and weight data during walking into multiple gait cycle phases and extracted both time-domain features—such as stride length and step width—and frequency-domain features—such as the spectral centroid. Features with a VIF greater than 10 were excluded, and a random-forest classifier was employed to identify 31 participants, achieving an $F1$-score of 0.918, as shown in Table II.

Because the walking path provided by our floor-based device was limited, the number of steps recorded on the plate varied across participants. To assess whether this hardware constraint affects the identification accuracy, we re-evaluated the model after removing the eight participants who produced an entire stride. As shown in Table III, the SVC with an RBF kernel achieved an $F1$-score of 0.930 and the random-forest classifier reached 0.924, which were approximately equivalent to those obtained with the full dataset and simply increased due to the reduced number of classes. These results suggest that our sensing approach can identify individuals with high accuracy even when only a single-step segment is available.

Conventional personal identification methods often rely on video imagery captured by cameras. However, these approaches pose risks of privacy violations due to facial reflections and are vulnerable to variations in clothing, hairstyle, light of environment, and capture angles [13], [15], [55], [58]. In contrast, the proposed method identifies individuals using CoG and weight data measured with a floor-based device, making it inherently robust against environmental lighting conditions and pedestrian appearance changes, while also being privacy-preserving.

Biometric identification, regardless of sensing modality, inevitably carries the risk of re-identification once the data are leaked, and the same holds for the CoG and weight signals used in this study. Nonetheless, CoG/weight data fundamentally differ from camera imagery in that they contain no visual information such as faces or silhouettes, which can be directly interpreted or reconstructed by humans. Moreover, camera systems can capture a wide field of view and often record high-granularity information from unintended third parties, depending on the system placement. In contrast, a floor-based sensor is inherently confined to specific transit points and acquires only the motion data required for identification, making the inadvertent collection of extraneous personal information far less likely. Consequently, the proposed floor-based approach offers a more privacy-favorable data footprint than vision-dependent methods. In addition, users are generally less aware of being "watched" by floor-based sensing than by cameras, and camera surveillance tends to be perceived unfavorably by end users [23], [42].

Several alternative privacy-preserving approaches, such as those using ToF sensors [54], triboelectric-based floor sensors [43], wearable accelerometers [10], Wi-Fi [50], and acoustics [56], have been explored. However, many of these methods target fewer than ten individuals. Our results demonstrate comparable or superior accuracy even for larger groups. Table VI lists the comparisons of the proposed method with related approaches, excluding camera-based systems. Because the studies listed in Table VI differ in sensor modality, cohort size, and walking conditions, their accuracy values cannot be strictly compared. Even so, the proposed low-density floor sensing system, equipped with only eight load cells, achieves an accuracy of 91.9% on a 31-participant dataset, demonstrating performance that is at least on par with existing nonvisual methods.

Given that individual identification is a 31-class classification task with a chance level of approximately 3.2%, achieving over 90% identification accuracy using only low-dimensional and abstract features like CoG and weight is notable. All participants were approximately 20 years old, with minimal age variation. Prior studies [27] have demonstrated that gait changes with age, indicating that the proposed method captures intrinsic, individual-specific gait characteristics. In addition, identification accuracy improved as the number of participants decreased (99.1% for three users, 97.4% for five users, and 96.4 % for ten users), highlighting the method's practicality in small-scale environments such as households. However, as illustrated in Fig. 9, the proposed system still exhibits an EER of approximately 20%. This level implies a nonnegligible probability of falsely accepting unregistered users. A promising way to reduce EER is to enlarge the training cohort, especially by incorporating participants across a wider age range and physiques, to increase interparticipant distances in the feature space and thereby improve open-set authentication performance.

TABLE VI
COMPARISON OF THE PROPOSED METHOD WITH NONVISUAL RELATED WORK. ACCURACY IS REPORTED AS IS IN EACH PAPER; DATASETS, WALKING CONDITIONS, AND SENSOR DENSITIES DIFFER. *N* IS THE NUMBER OF PARTICIPANTS

Method	Data Type	Samples	N	Accuracy
This paper	Weight/CoG	80	31	91.9 %
			10	96.4 %
	CoG only		31	82.0 %
			10	91.2 %
[56]	Acoustic	96.6 %	40–60	50
[50]	Wi-Fi	93.1 %	50–60	50
[43]	Triboelectric	96.0 %	100	10
[54]	Distance	91.1 %	10	10
[10]	Acceleration	95.0 %	12	5

Fig. 10 shows that identification stability is lower when the number of samples per individual is 10 compared with when it is 20 or more. Therefore, it is crucial to ensure a sufficient number of samples (20 or more) for practical applications.

2) Robustness to External Disturbance: As shown in Table IV, the proposed system maintained high identification accuracy even when participants carried luggage. In the experiment, 19 of the 31 participants carried backpacks, while 11 carried tote bags, shoulder bags, or other types of luggage, which caused the CoG to shift to one side of the body (the luggage was carried in by each participant, with handle positions varying by individual). In other words, even though the data varied widely across participants depending on the type of luggage, the gait characteristics originating from the individuals were consistently captured in a robust manner.

In conventional gait identification using video images, the effects of the user's clothing, hairstyle, luggage, and other factors have been problematic [13], [15], [55], [58]. However, the CoG and weight data are not affected by lighting conditions or occlusion on the screen, and as mentioned above, they are also less influenced by luggage. Therefore, the system is more robust to noise caused by the user and the environment than existing systems, and the results shown in Table IV support this. However, the CoG and weight data may be affected by the type of shoe, although the effects of clothing and hairstyle are minimal. Of the 31 participants in the experiment, 24 participants wore sneakers, whereas only three participants wore shoes such as high heels or sandals, which influenced the CoG shift. Therefore, it is necessary to verify the accuracy of identification when the same person wears different types of shoes and to investigate the effect of shoe type on identification in future studies.

In vision-based methods, many studies use GEI/silhouette inputs; carried objects act as external disturbances that alter the silhouette and have been reported to degrade accuracy or require condition-specific countermeasures [25], [60]. Similarly, pressure-sensor approaches have reported performance drops under carried-object conditions [53]. A plausible mechanism is that pipelines treating the pressure map as an image often depend on absolute distributions and spatial alignment; thus, load offsets induced by the object and the associated postural change can directly translate into pattern differences, thereby reducing performance.

In contrast, our system measures only the board-level CoG and total vertical load and, via ROGA-aligned feature extraction with standardized, relative-oscillation features, captures individual-specific gait patterns while absorbing offsets due to carrying. Accordingly, in our dataset, the identification performance under carried-object perturbations was practically unchanged ($F1$-score $= 0.918$).

Nevertheless, extremely heavy or markedly asymmetric loads may still affect performance, and systematic evaluation under such conditions is left for future work.

3) Identification Using CoG Oscillation Only: To further reduce privacy concerns, we explored identification using only CoG oscillation data, excluding weight data. Although performance dropped, achieving an $F1$-score of 0.817 for 31 participants (see Table V) demonstrates that CoG oscillation alone captures meaningful individual-specific gait patterns. This finding suggests the feasibility of developing highly privacy-conscious identification systems.

Table VI also lists the comparison of the identification accuracy of the CoG-only mode with that reported by several nonvisual approaches. When 31 participants are involved, the CoG-only accuracy is lower than that of any reference method, and as a blurred facial image becomes harder for humans to recognize, the lucking of load information increases privacy, but inevitably costs accuracy. In other words, the CoG/weight modality exhibits an inherent privacy–accuracy tradeoff: the higher the abstraction level, the greater the loss of discriminative power.

In contrast, when the task was restricted to ten participants, the CoG-only mode attained an accuracy of 91.2%, marginally exceeding that of the prior work [54]. This indicates that although accuracy declines with larger cohorts, the CoG-only configuration can still deliver acceptable performance in use cases that involve a limited number of users.

4) Analyzing Key Features for Identification: Although this study achieved highly accurate individual identification, principal component analysis (PCA) was performed to evaluate which features contributed to the identification. As a result, the contribution of the first principal component was approximately 13%. To achieve a cumulative contribution exceeding 90%, up to the 20th principal component was required. This suggests that no single feature is heavily biased toward a specific principal component and that the information is distributed across multiple dimensions, making dimensionality reduction challenging. Given the structure of the information distributed across many principal components and the high accuracy of the identification results, the feature groups extracted in this study effectively and independently represented the individual gait characteristics. Therefore, the feature design and selection in this study can be considered appropriate.

To validate this consideration, the contribution of each feature was investigated. However, determining the contribution of individual features from the loadings of the principal components is challenging because many principal components have low contribution rates. Therefore, in this study, the permutation importance of each feature is calculated.

Figs. 11 and 12 show the permutation importance of each feature.

These analyses show that the contributions of the features corresponding to LR and PSw are high for $\mu_{X,\mathrm{LR}}$, $\mu_{W,\mathrm{LR}}$, $\mu_{W,\mathrm{PSw}}$, and $\sigma_{W,\mathrm{LR}}$, regardless of the presence of weight data. Both LR and PSw represent the time periods from when the heel of one foot makes contact with the ground until the opposite foot lifts off, suggesting that individual characteristics are relatively strongly expressed during the shift of the CoG from one foot to the other. In particular, the CoG shift from foot to foot is thought to depend on the stepping motion of the rear foot, with individual differences being strongly reflected in the CoG oscillation and the force applied during the stepping motion.

The LR phase, as defined in ROGA, is mainly responsible for weight acceptance, a function that requires coordination of the hip and knee joints. Biomechanically, co-contraction of the quadriceps and hamstring muscles stabilizes these joints [6]; in addition, the gluteus maximus also controls hip flexion, thereby enhancing pelvic stability [52].[1] Consequently, interindividual differences in the size and flexibility of these muscle groups may manifest in CoG oscillations and weight shifts, potentially explaining the high permutation importance of features such as $\mu_{X,\mathrm{LR}}$ and $\mu_{W,\mathrm{PSw}}$. Winter [52] also reported relatively high EMG activity of the erector-spinae (ES) muscles during both LR and PSw. Because the ES contributes to trunk rotational control during gait [52], individual variations in trunk stability could influence the identification performance. Postural habits such as thoracic kyphosis or habitual forward/backward lean might likewise affect the CoG trajectory, and these effects may be linked to the functional state of ES.

In contrast, although TSt is defined in this article as the phase of transition from step-off to the next step, most of the features in TSt are excluded based on the VIF threshold, and the contribution of the remaining features is also low. This contrasts with the high contribution of the features corresponding to LR and PSw, indicating that there is room for improvement in the process of extracting the gait cycle from the CoG and weight data based on the ROGA. Therefore, a more detailed understanding of the CoG oscillation and the directional force of the footsteps, along with a more appropriate alignment with the CoG and weight data, is expected to further improve individual identification performance.

Furthermore, when frequency features were extracted in this study, as reported in previous studies [41], all of these features remained without being excluded by the VIF, indicating that each frequency feature independently retains valuable information. On the other hand, permutation importance analysis revealed that maximum power features, such as P_X, and the spectral centroid of gravity, such as C_X, had relatively high contributions, whereas spectral flatness features, such as F_X, showed almost 0 or negative contributions. This suggests that individual differences exist in the rhythm of gait and that the magnitude and bias of the dominant frequency components

[1]This citation refers to the first edition of the book (1987). A revised edition titled "The Biomechanics and Motor Control of Human Gait: Normal, Elderly and Pathological" was later published in 1991.

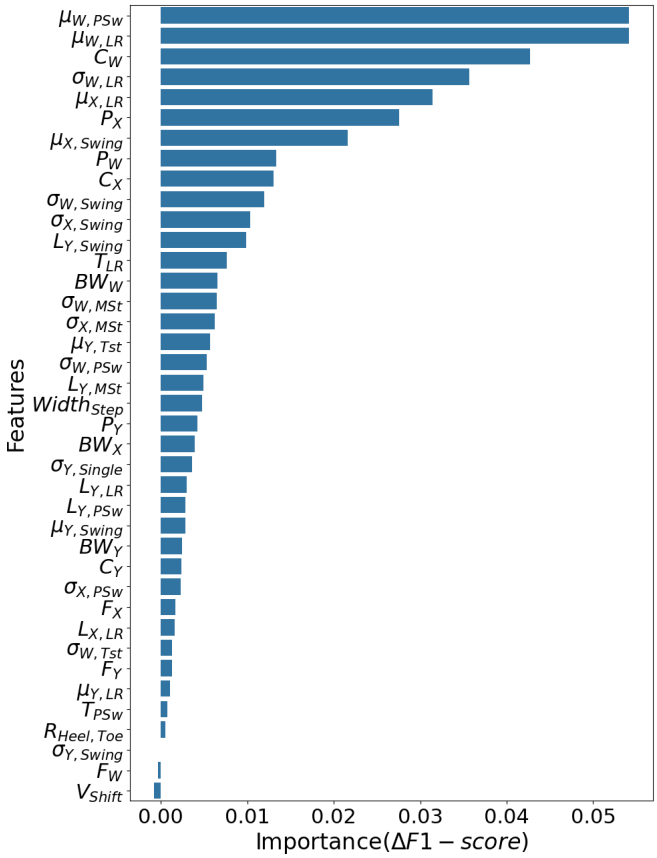

Fig. 11. Permutation importance (with weight data).

are effective for discrimination, whereas spectral flatness tends to fluctuate from gait to gait and is unlikely to contribute to individual discrimination.

Although high-accuracy deep learning pipelines are widely used in floor-based approaches [43], designs that make phasewise (gait phase) feature contributions explicit are not common in these approaches. In contrast, our study combines ROGA comply phase segmentation and phase-specific feature design with permutation importance-based analysis, yielding empirical insight into which phases—particularly LR and PSw—contribute to individual identification.

B. Limitation and Future Work

Whereas the proposed system exhibited robustness to luggage variations, only one type of luggage was used per participant. In real-world scenarios, people change bags and clothing depending on the situation, such as temperature, mood, or destination. Future work should include data from the same individuals carrying various types of luggage to build models that are truly invariant to such variations. Similarly, because only a limited range of footwear was tested—24 participants wore sneakers and 3 wore high heels or sandals—future studies should verify identification accuracy for the same individual wearing different shoe types to assess any impact on CoG shift and recognition performance. Expanding the dataset to include participants of different ages and genders will also enable broader application beyond individual identification, including attribute estimation such as age, gender, or health status.

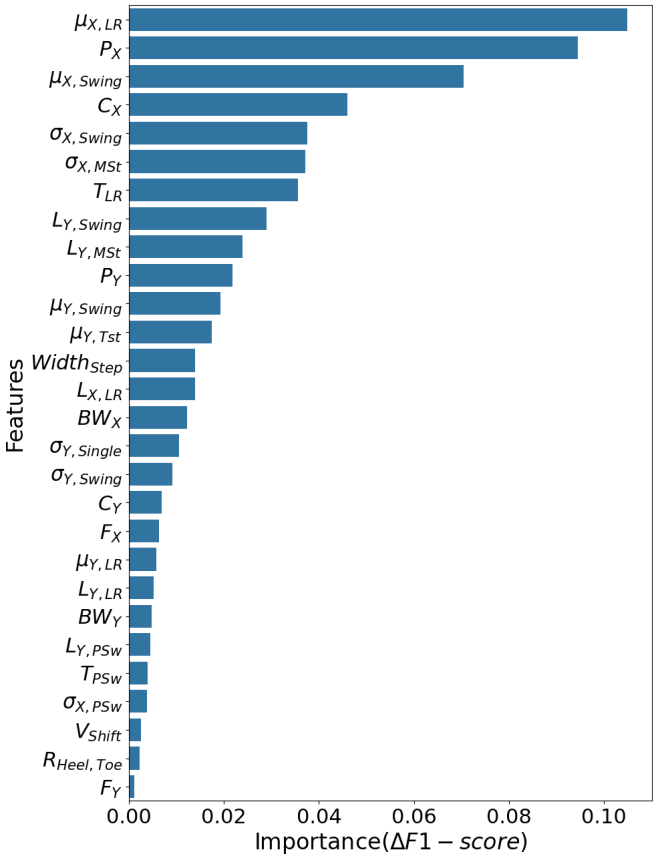

Fig. 12. Permutation importance (without weight data).

Although this system is less affected by the noise caused by clothes or luggage, the effects of the angle and direction of walking on the device remain unresolved. We aim to address these problems by exploring approaches, such as developing an algorithm that accounts for the direction of walking or measuring and analyzing gait during turns. In addition, the floor-based device developed in this study, with its simple and low-cost configuration, makes it difficult to support the simultaneous identification of multiple individuals. Whereas there are some potential solutions, such as installing the device in application scenarios where only one person passes through at a time, such as at station ticket gates, this is not an inherent solution, but a hardware limitation.

When the system is deployed in real-world settings, the boundary between the floor-based device and the surrounding floor can draw users' attention and unintentionally alter their gaits. To avoid such artifacts, the platform should be integrated seamlessly, for example, by matching the floor finish or overlaying the plate with the same laminate, vinyl, or carpet used elsewhere. As part of our future work, we plan to examine: 1) how different device–floor interfaces influence walking behavior and 2) how additional surface materials placed on the plate affect identification accuracy, which remains to be investigated in future work.

In this study, we adopted conventional feature extraction and feature contribution analyses to investigate both the identification capability and interpretability of features derived from low-density floor-sensor data, namely, the CoG trajectory and the vertical ground-reaction force recorded during walking. As shown in Section V-A4, the load-acceptance pattern that occurs during foot strike exhibits pronounced interindividual differences, accounting for a large share of the model's discriminative power. Building on this finding, our future work will focus on developing a sensing system that can capture this load-transfer signature with higher precision, thereby further improving the identification performance.

The current device can only measure the coordinates of the CoG and the vertical component of the ground force; it cannot record the shear forces or moment of the vertical axis (free moment) generated during foot strike. A commercial six-DOF force plate [45] can capture the full six-component force/moment vector at the foot–floor interface, which has proven to be valuable for assessing health status and disease [7], [30]. However, force plates are prohibitively expensive to deploy in homes or small facilities. Therefore, we plan to explore low-cost sensor configurations and signal-reconstruction techniques capable of estimating six-axis force information with the aim of achieving more detailed and interpretable gait sensing at a fraction of the cost.

C. Threat Model

In this study, "privacy-preserving" means that even if data are unintentionally disclosed due to external attack, insider misconduct, or operational error, the recorded signals do not readily enable direct re-identification of specific individuals from human-interpretable appearance cues (e.g., face and silhouette/body shape). The implemented floor-based device acquires only nonvisual, low-dimensional signals—CoG (X, Y) and vertical load (W)—only while a person traverses a confined sensing area of 1.5 × 0.9 m (1.35 m^2), thereby structurally limiting both the representational content (visualization of appearance) and capture scope (incidental bystanders). In contrast, vision-based methods, while accurate, tend to include human-interpretable appearance cues by design and, upon leakage, may incur a relatively higher reidentification risk through cross referencing with external information.

However, residual risks remain as general constraints in biometrics. For example, if an adversary already possesses a labeled template set collected with the same class of device, within-set reidentification may be possible. Accordingly, for system operation in the wild, we recommend data minimization (including an optional CoG-only mode), local isolation/pseudonymization, short retention of raw data with feature-only storage thereafter, and key management.

D. Application Scenarios

The proposed method has several potential applications. Focusing on personal identification, the proposed method can replace conventional systems installed in areas such as homes and offices, where only specific users interact with the system. It allows for smoother entry and exit compared with existing object-based methods that rely on cards or real keys. In particular, when the number of people to be identified was 10 or fewer, 15 samples were identified with an $F1$-score of 0.90 or higher, and 40 samples were identified with an $F1$-score of 0.95 or higher. Accuracy can improve over time as

users walk on a floor-based device daily. The user only needs to consciously register data during the initial enrollment, after which they can unconsciously benefit from the gait analysis system by simply going about their normal activities. The ability to identify users enables the detection of suspicious unregistered individuals. Moreover, floor-sensor methods, such as the one used in this study, can not only identify who is walking but also track their location within a building. By installing multiple floor-based devices, a floor-sensor network can be created, allowing monitoring of who walks on which device. This could be particularly useful for managing individuals who require care or who tend to wander. Whereas this study focused on individual identification, we believe that gender and age can also be determined using the proposed method. If gender and age can be identified, the system could be deployed in high-traffic areas, such as ticket gates and mall entrances and applied in marketing, such as human flow analysis targeting a large, unspecified group of people.

However, as illustrated in Fig. 9, the current prototype still yields a comparatively high EER, implying a residual risk of falsely accepting suspicious, unregistered users. To make the system viable for intrusion-detection scenarios, the training dataset must be expanded and diversified, for example, by including users across a much broader age range, so that inter-participant distances in the feature space increase and the EER can be driven down.

We also believe that it is possible to evaluate health status and predict specific diseases by observing the swaying of the CoG during movements in daily life. By using a gait analysis system to monitor specific users over time, we hope to track changes in leg strength and unconsciously monitor the elderly, thereby contributing to the extension of their healthy life expectancy.

VI. Conclusion

We developed a floor-based device capable of sensing CoG and weight data in a low-dimensional, abstract, and privacy-preserving manner, and proposed a gait analysis system for individual identification. Leveraging the ROGA system as a reference for gait cycle segmentation, we extracted both time-domain and frequency-domain features from the walking data.

Using stratified fivefold cross validation, we achieved an $F1$-score of 0.918 in identifying 31 participants. Notably, even when weight data were excluded, the system attained an $F1$-score of 0.817, demonstrating that individual characteristics could be extracted from CoG oscillation alone, rather than relying solely on weight. Moreover, for small-scale deployments involving about ten users, the $F1$-score marked above 0.90, underscoring the method's practicality in household-sized scenarios. Finally, the feature contribution analysis revealed that individual differences were particularly pronounced during the step-off phase of walking.

Because the proposed method utilizes only abstract CoG and weight data, it can provide enhanced privacy protection relative to camera-based and many other conventional approaches, while maintaining stable identification during natural, everyday walking. The system is also expected to be robust to variations such as clothing, hairstyle, ambient lighting, and even the presence of luggage. In addition, the hardware implementation was maintained simple; eight load cells were mounted on a 150 × 90 cm aluminum plate. This configuration is less expensive than commercially available six-DOF force plates and, unlike high-density pressure mats reported in previous studies, requires only a one-time coarse calibration and no sensor-by-sensor fine-tuning, unlike high-density pressure mats. Combined with its inherent immunity to occlusion problems that plague camera-based systems, the proposed platform offers a practical, low-cost, and privacy-conscious alternative for real-world deployment.

In future work, we plan to build a more general and highly accurate dataset by collecting data across a wide range of conditions, including various clothing styles, footwear, and types of luggage, from a diverse group of individuals of different ages and genders. This expansion will facilitate not only individual identification but also the estimation of attributes, such as gender, age, and health status.

Additionally, to further improve identification accuracy, we aim to develop a low-cost gait sensing method capable of measuring not only vertical load and CoG position but also 3-D forces and torques around each axis.

This research enables individual identification in environments that closely resemble everyday walking, and holds promise for applications in medicine, marketing, and beyond, as a privacy-conscious alternative to conventional systems.

References

[1] *Rancho Los Amigos National Rehabilitation Center*. Accessed: Jan. 24, 2025. [Online]. Available: https://dhs.lacounty.gov/rancho/

[2] A&D. *LCB03*. Accessed: Jan. 10, 2023. [Online]. Available: https://www.aandd.jp/products/weighing/loadcell/lcb03.html

[3] B. Arnrich, C. Setz, R. La Marca, G. Tröster, and U. Ehlert, "What does your chair know about your stress level?" *IEEE Trans. Inf. Technol. Biomed.*, vol. 14, no. 2, pp. 207–214, Mar. 2010, doi: 10.1109/TITB.2009.2035498.

[4] I. Bouchrika, M. Goffredo, J. Carter, and M. Nixon, "On using gait in forensic biometrics," *J. Forensic Sci.*, vol. 56, no. 4, pp. 882–889, Jul. 2011.

[5] A. Bränzel et al., "GravitySpace: Tracking users and their poses in a smart room using a pressure-sensing floor," in *Proc. SIGCHI Conf. Hum. Factors Comput. Syst.*, 2013, pp. 725–734.

[6] R. Brunner and E. Rutz, "Biomechanics and muscle function during gait," *J. Children's Orthopaedics*, vol. 7, no. 5, pp. 367–371, Nov. 2013.

[7] G. Dalleau, M. S. Allard, M. Beaulieu, C.-H. Rivard, and P. Allard, "Free moment contribution to quiet standing in able-bodied and scoliotic girls," *Eur. Spine J.*, vol. 16, no. 10, pp. 1593–1599, Oct. 2007.

[8] F. Delaine, B. Lebental, and H. Rivano, "In situ calibration algorithms for environmental sensor networks: A review," *IEEE Sensors J.*, vol. 19, no. 15, pp. 5968–5978, Aug. 2019.

[9] Y. Dong and H. Y. Noh, "Ubiquitous gait analysis through footstep-induced floor vibrations," *Sensors*, vol. 24, no. 8, p. 2496, Apr. 2024.

[10] M. Fujii, K. Kato, C. Xia, and Y. Sugiura, "Personal identification using gait data on slipper-device with accelerometer," in *Proc. Asian CHI Symp.*, May 2021, pp. 74–79.

[11] M. Gadaleta and M. Rossi, "IDNet: Smartphone-based gait recognition with convolutional neural networks," *Pattern Recognit.*, vol. 74, pp. 25–37, Feb. 2018.

[12] D. Gafurov, "A survey of biometric gait recognition: Approaches, security and challenges," in *Proc. Annu. Norwegian Comput. Sci. Conf.*, 2007, pp. 19–21.

[13] M. A. Hossain, Y. Makihara, J. Wang, and Y. Yagi, "Clothing-invariant gait identification using part-based clothing categorization and adaptive weight control," *Pattern Recognit.*, vol. 43, no. 6, pp. 2281–2291, Jun. 2010.

[14] H. Iwama, D. Muramatsu, Y. Makihara, and Y. Yagi, "Gait verification system for criminal investigation," *Inf. Media Technol.*, vol. 8, no. 4, pp. 1187–1199, 2013.

[15] H. Iwama, M. Okumura, Y. Makihara, and Y. Yagi, "The OU-ISIR gait database comprising the large population dataset and performance evaluation of gait recognition," *IEEE Trans. Inf. Forensics Security*, vol. 7, no. 5, pp. 1511–1521, Oct. 2012.

[16] M. J. Perry, "Gait analysis: Normal and pathological function," SLACK, Pitman, NJ, USA, Tech. Rep., 2010.

[17] A. Jain, L. Hong, and S. Pankanti, "Biometric identification," *Commun. ACM*, vol. 43, no. 2, pp. 90–98, Feb. 2000, doi: 10.1145/328236.328110.

[18] A. K. Jain, A. Ross, and S. Prabhakar, "An introduction to biometric recognition," *IEEE Trans. Circuits Syst. Video Technol.*, vol. 14, no. 1, pp. 4–20, Jan. 2004, doi: 10.1109/TCSVT.2003.818349.

[19] A. P. Kaur, E. Nsugbe, A. Drahota, M. Oldfield, I. Mohagheghian, and R. A. Sporea, "State-of-the-art fall detection techniques with emphasis on floor-based systems—A review," *Biomed. Eng. Adv.*, vol. 9, Jun. 2025, Art. no. 100179.

[20] J. H. Kim, "Multicollinearity and misleading statistical results," *Korean J. Anesthesiology*, vol. 72, no. 6, pp. 558–569, Dec. 2019, doi: 10.4097/kja.19087.

[21] T. Kitabayashi, S. Demura, and H. Murase, "Proposal for a new body sway evaluation method," *Perceptual Motor Skills*, vol. 113, no. 1, pp. 127–138, Aug. 2011.

[22] J. R. Kwapisz, G. M. Weiss, and S. A. Moore, "Cell phone-based biometric identification," in *Proc. 4th IEEE Int. Conf. Biometrics, Theory, Appl. Syst. (BTAS)*, Sep. 2010, pp. 1–7.

[23] G. Laput, Y. Zhang, and C. Harrison, "Synthetic sensors: Towards general-purpose sensing," in *Proc. CHI Conf. Human Factors Comput. Syst.*, May 2017, pp. 3986–3999.

[24] P. K. Larsen, E. B. Simonsen, and N. Lynnerup, "Gait analysis in forensic medicine," *J. Forensic Sci.*, vol. 53, no. 5, pp. 1149–1153, 2008.

[25] X. Li, Y. Makihara, C. Xu, Y. Yagi, and M. Ren, "Gait recognition invariant to carried objects using alpha blending generative adversarial networks," *Pattern Recognit.*, vol. 105, Sep. 2020, Art. no. 107376.

[26] N. Lynnerup and P. K. Larsen, "Gait as evidence," *IET Biometrics*, vol. 3, no. 2, pp. 47–54, 2014.

[27] Y. Makihara, H. Mannami, and Y. Yagi, "Gait analysis of gender and age using a large-scale multi-view gait database," in *Proc. 10th Asian Conf. Comput. Vis.*, 2011, pp. 440–451.

[28] S. Mei et al., "High-density, highly sensitive sensor array of spiky carbon nanospheres for strain field mapping," *Nature Commun.*, vol. 15, no. 1, p. 3752, May 2024.

[29] L. Middleton, A. A. Buss, A. Bazin, and M. S. Nixon, "A floor sensor system for gait recognition," in *Proc. 4th IEEE Workshop Autom. Identificat. Adv. Technol. (AutoID)*, May 2005, pp. 171–176.

[30] C. E. Milner, I. S. Davis, and J. Hamill, "Free moment as a predictor of tibial stress fracture in distance runners," *J. Biomechanics*, vol. 39, no. 15, pp. 2819–2825, Jan. 2006.

[31] R. Miyazaki, K. Sasaki, N. Tsumura, and K. Hirai, "Hand authentication from RGB-D video based on deep neural network," *Electron. Imag.*, vol. 34, no. 17, pp. 1–5, Jan. 2022.

[32] Y. Nakamura, K. Ito, T. Hasegawa, S. Itami, Y. Saika, and M. Nakagawa, "Individual identification by gait vibration data transmitted floor," in *Proc. 16th Int. Conf. Control, Autom. Syst. (ICCAS)*, Oct. 2016, pp. 1371–1376.

[33] A. Nambiar, A. Bernardino, and J. C. Nascimento, "Gait-based person re-identification: A survey," *ACM Comput. Surveys*, vol. 52, no. 2, pp. 1–34, Mar. 2020.

[34] B. News. *How Can You Identify a Criminal by the Way They Walk?*. Accessed: Jan. 10, 2023. [Online]. Available: http://news.bbc.co.uk/2/hi/uk_news/magazine/7348164.stm

[35] K. Nishimura, K. Ito, K. Fujiwara, K. Fujita, and Y. Itoh, "Detection of nodding of interlocutors using a chair-shaped device and investigating relationship between a divergent thinking task and amount of nodding," *Qual. User Exper.*, vol. 8, no. 1, p. 10, Dec. 2023.

[36] R. J. Orr and G. D. Abowd, "The smart floor: A mechanism for natural user identification and tracking," in *Proc. CHI Extended Abstr. Human Factors Comput. Syst.-CHI*, 2000, pp. 275–276.

[37] R. Ozaki et al., "Frailty assessment using a floor panel-type device by measuring center of pressure," *Proc. ACM Interact., Mobile, Wearable Ubiquitous Technol.*, vol. 8, no. 4, pp. 1–27, Nov. 2024.

[38] M. Pavlou and N. M. Allinson, "Automatic extraction and classification of footwear patterns," in *Proc. Int. Conf. Intell. Data Eng. Automated Learn.*, 2006, pp. 721–728.

[39] T. Randhavane et al., "Learning gait emotions using affective and deep features," in *Proc. 15th ACM SIGGRAPH Conf. Motion, Interact. Games*, Nov. 2022, pp. 1–10, doi: 10.1145/3561975.3562957.

[40] N. K. Ratha, J. H. Connell, and R. M. Bolle, "Enhancing security and privacy in biometrics-based authentication systems," *IBM Syst. J.*, vol. 40, no. 3, pp. 614–634, 2001.

[41] E. Sejdic, K. A. Lowry, J. Bellanca, M. S. Redfern, and J. S. Brach, "A comprehensive assessment of gait accelerometry signals in time, frequency and time-frequency domains," *IEEE Trans. Neural Syst. Rehabil. Eng.*, vol. 22, no. 3, pp. 603–612, May 2014.

[42] K. Seymour, J. McNicoll, and R. Koenig-Robert, "Big brother: The effects of surveillance on fundamental aspects of social vision," *Neurosci. Consciousness*, vol. 2024, no. 1, Dec. 2024, Art. no. niae039.

[43] Q. Shi et al., "Deep learning enabled smart mats as a scalable floor monitoring system," *Nature Commun.*, vol. 11, no. 1, p. 4609, Sep. 2020.

[44] J. F. Stins, A. Ledebt, C. Emck, E. H. van Dokkum, and P. J. Beek, "Patterns of postural sway in high anxious children," *Behav. Brain Functions*, vol. 5, no. 1, p. 42, 2009.

[45] L. Tec Gihan Co. *Force Plate*. Accessed: May 25, 2025. [Online]. Available: https://tecgihan.co.jp/en/product/forceplate/

[46] B. Toro, C. Nester, and P. Farren, "A review of observational gait assessment in clinical practice," *Physiotherapy Theory Pract.*, vol. 19, no. 3, pp. 137–149, Jan. 2003.

[47] S. C. Walpole, D. Prieto-Merino, P. Edwards, J. Cleland, G. Stevens, and I. Roberts, "The weight of nations: An estimation of adult human biomass," *BMC Public Health*, vol. 12, no. 1, pp. 1–6, Dec. 2012.

[48] C. Wan, L. Wang, and V. V. Phoha, "A survey on gait recognition," *ACM Comput. Surv.*, vol. 51, no. 5, pp. 1–35, 2018.

[49] T. Wang et al., "A gait assessment framework for depression detection using Kinect sensors," *IEEE Sensors J.*, vol. 21, no. 3, pp. 3260–3270, Feb. 2021.

[50] W. Wang, A. X. Liu, and M. Shahzad, "Gait recognition using WiFi signals," in *Proc. ACM Int. Joint Conf. Pervasive Ubiquitous Comput.*, 2016, pp. 363–373.

[51] P. Welch, "The use of fast Fourier transform for the estimation of power spectra: A method based on time averaging over short, modified periodograms," *IEEE Trans. Audio Electroacoustics*, vol. AU-15, no. 2, pp. 70–73, Jun. 1967.

[52] D. A. Winter, *Biomechanics and Motor Control of Human Gait*. Waterloo, ON, Canada: Univ. Waterloo Press, 1987.

[53] C.-C. Wu, C.-W. Tsai, F.-E. Wu, C.-H. Chiang, and J.-C. Chiou, "Plantar pressure-based gait recognition with and without carried object by convolutional neural network-autoencoder architecture," *Biomimetics*, vol. 10, no. 2, p. 79, Jan. 2025.

[54] C. Xia, A. Munakata, and Y. Sugiura, "Privacy-aware gait identification with ultralow-dimensional data using a distance sensor," *IEEE Sensors J.*, vol. 23, no. 9, pp. 10109–10117, May 2023.

[55] C. Xu et al., "Real-time gait-based age estimation and gender classification from a single image," in *Proc. IEEE/CVF Winter Conf. Appl. Comput. Vis.*, Jan. 2021, pp. 3460–3470.

[56] W. Xu, Z. Yu, Z. Wang, B. Guo, and Q. Han, "AcousticID: Gait-based human identification using acoustic signal," *Proc. ACM Interact., Mobile, Wearable Ubiquitous Technol.*, vol. 3, no. 3, pp. 1–25, Sep. 2019.

[57] T. Yoshida, N. Okazaki, K. Takaki, M. Hirose, S. Kitagawa, and M. Inami, "Flexel: A modular floor interface for room-scale tactile sensing," in *Proc. 35th Annu. ACM Symp. User Interface Softw. Technol.*, Oct. 2022, pp. 1–12.

[58] S. Yu, D. Tan, and T. Tan, "Modelling the effect of view angle variation on appearance-based gait recognition," in *Proc. Comput. Vis.-ACCV*, 2006, pp. 807–816.

[59] T. Yu, H. Jin, and K. Nahrstedt, "ShoesLoc: In-shoe force sensor-based indoor walking path tracking," *Proc. ACM Interact., Mobile, Wearable Ubiquitous Technol.*, vol. 3, no. 1, pp. 1–23, Mar. 2019.

[60] Z. Zhang et al., "Gait recognition via disentangled representation learning," in *Proc. Conf. Comput. Vis. Pattern Recognit.*, Jun. 2019, pp. 4710–4719.